Nanoscale

Accepted Manuscript

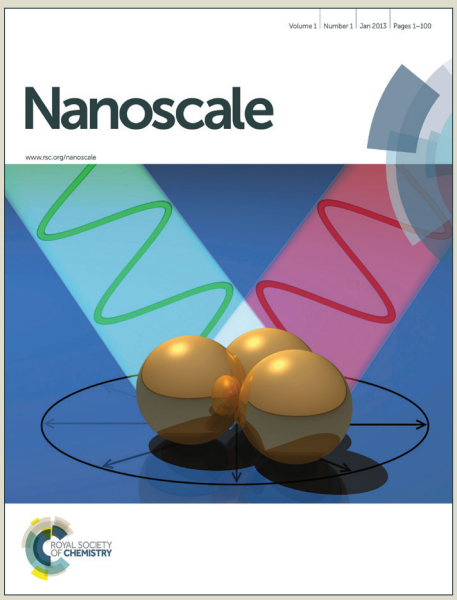

ROYAL SOCIETY OF CHEMISTRY

www.rsc.org/nanoscale

Cite this: DOI: 10.1039/c0xx00000x

www.rsc.org/xxxxxx

ARTICLE TYPE

Cobalt-Nitrogen Complex on N-doped Three-Dimensional Graphene framework as Highly Efficient Electrocatalysts for Oxygen Reduction Reaction

Yuanyuan Jiang,[a,c] Yizhong Lu,[a,c] Xiaodan Wang,[a] Yu Bao,*[b] Wei Chen,[a] and Li Niu*[a]

Received (in XXX, XXX) Xth XXXXXXXXX 20XX, Accepted Xth XXXXXXXXX 20XX
DOI: 10.1039/b000000x

The high cost and limited natural abundance of platinum hinder its widespread applications as the oxygen reduction reactions (ORR) electrocatalyst for fuel-cells. Carbon-supported materials containing metals such as Fe or Co as well as nitrogen have been proposed to reduce the cost without obvious lowering of the performance compared to Pt-based electrocatalysts. In this work, based on the pyrolyzed corrin structure of vitamin B12 on simultaneously reduced graphene support (g-VB12), we constructed an efficient oxygen reduction electrocatalysts with very positive half-wave potential (only ~ 30 mV deviation from Pt/C), high selectivity (electron transfer number close to 4) and excellent durability (only 11 mV shift of half-wave potential after 10000 potential cycles). The admirable performance of this electrocatalyst can be attributed to its homogeneous distribution of abundant Co-N_x active sites, and well-defined three-dimensional mesoporous structure of the N-doped graphene support. The high activity and long-term stability of the low cost g-VB12 make it a promising ORR electrocatalyst in alkaline fuel cells.

Introduction

Electrochemical energy conversion and storage devices, ranging from fuel cells to metal-air batteries, require effective cathodic electrocatalysts for promoting the sluggish oxygen reduction reaction (ORR).[1,2] Pt and Pt-based materials remain the most efficient ORR catalysis by far, but the high cost and scarcity in earth of Pt greatly hamper its further development for large-scale applications.[3,4] In this respect, a broad range of catalysts based on nonprecious metals or metal oxides (Fe, Co, etc. or Fe_3O_4, CoO, Co_3O_4, IrO_2, etc.),[5-8] nitrogen doped carbon materials (carbon nanotubes, graphene materials, carbon nanoparticles, etc.),[9-12] as well as nitrogen-coordinated transition metals supported on carbon hybrid materials (M-N_x) have been actively researched as ORR electrocatalysts.[13-15] Among those reported approaches, pyrolysis of nitrogen coordinated Fe or Co complex (such as porphyrins and phthalocyanine) supported on carbon has been established as one of the most promising non-precious metal electrocatalysts.[16,17] Since 1964, when Jasinski demonstrated that cobalt phthalocyanine could act as ORR electrocatalyst,[18] various metal-N_4 complexes supported on carbon were exploited. However, stability issues arose as the catalyst structure tended to decompose during the testing process, leading to the loss of catalytic activity.[19,20] A significant breakthrough was achieved years later by pyrolyzing the Fe-N_4 or Co-N_4 macrocycles on the carbon support in an inert atmosphere.[21,22] The resulting catalyst demonstrated improved stability, whereas the high-price of these macrocycles hindered their broad application. It was proposed by some researchers that these expensive transition metal macrocycle compounds were actually not necessary, for the only requirement was a proper metal-nigrogen coordination supported on carbon resulting from heat treatment of transition metal, nitrogen and carbon precursor materials. To verify this, in 1989, one kind of promising ORR electrocatalysts with a M-Nx structure was successfully prepared by pyrolyzing polyacrylonitrile, Co or Fe salts, and a Vulcan XC-72 carbon black support.[23] Another breakthrough was achieved in 2009 when lefèvre's group produced microporous carbon supported Fe-Nx based catalysts by using Black Pearls 2000 as carbon support, FeAc as the iron precursor, and 1,10-phenanthroline as the N source. The ballmilling treated mixture was further subjected to heat treatment in ammonia, both as N source and to create porosity. The active sites were believed to be Fe cations coordinated by pyridinic nitrogen functionalities in the interstices of graphitic sheets within the micropores.[24] Even so, these methods also suffer from a dilemma that the metal may not be coordinated by N exactly according to the researches' intention.

An alternative way is raised by exploiting other low cost macrocycles materials with M-Nx center. Cyanocobalamin (Vitamin B12, VB12) with a corrin structure in the center (Co center coordinated by certain N atoms), is a porphyrin like structure, nevertheless, its cost is much lower than other macrocycles molecules such as porphyrins and phthalocyanines. And it can be easily obtained by mass production. In previous research, calculations based on density functional theory suggested that the corrin complex with a low-symmetric structure offered a much preferable ORR pathway, which is not applicable to the porphyrin molecule with a high symmetry.[25]

Herein, we develop a new type of ORR electrocatalyst based on this cheap and easily obtained VB12 as Co and N precursor

and reduced graphene oxide as the carbon support. After lyophilization and pyrolysis treatment of the VB12 and graphene oxide mixture, the as-prepared g-VB12 presents a 3D mesoporous structure with a relatively high Brunauer-Emmett-Teller (BET) surface area (ca. 220 m^2 g^{-1}). The g-VB12 exhibits higher activity and superior electrochemical durability than the pyrolyzed VB12 supported on carbon black (VB12/C) for the ORR in alkaline media. Additionally, the g-VB12 electrocatalyst outperforms the commercial Pt/C (20 wt % Pt) in durability and anti-poison capability in half cell test. The good electrocatalytic activity can be primarily attributed to the homogeneously dispersed Co-Nx active sites. While the three-dimensional mesoporous N-doped graphene framework of this g-VB12 offers the highly accessible surface area and an efficient mass transport as well as electron transfer path, also resulting in the improved ORR performance. The desirable performance of the g-VB12 electrocatalyst, together with the low cost of the easily obtained raw materials and the facile synthesis procedure, make the g-VB12 a promising cathode catalyst candidate for alkaline methanol fuel cell applications.

Results and Discussions

The structure and morphology of the as-fabricated g-VB12 were first studied by scanning electron microscopy (SEM). As can be seen from Figure 1, the g-VB12 exhibits an interconnected, three dimensional rough framework with continuous crumpled sheet structure, which is the typical feature of 3D graphene.[26,27] The adsorption surface area and the porosity of the g-VB12 are evaluated by N_2 adsorption measurements. As shown in Figure 1c and Figure 1d, the distinct hysteresis loops indicate the mesoporous texture with the uniform mesopore size distribution centered at 4.5 nm, according to the Barrett-Joyer-Halenda (BJH) model. The Brunauer-Emmett-Teller (BET) analysis shows a specific surface area of 220 m^2 g^{-1} for the g-VB12, which is relatively higher than that of the VB12/C with an aggregated spheres structure (105 m^2 g^{-1}, Figure S1). The highly accessible surface area and 3D mesoporous texture of the g-VB12 composite are beneficial to the transport of electron and materials, thus favourable for the electrocatalytic activity.

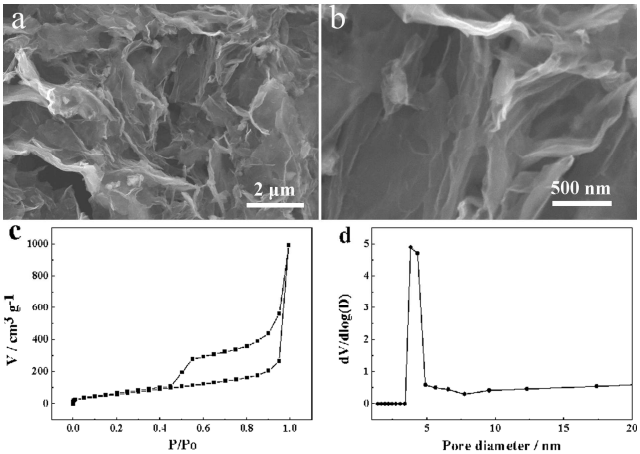

Figure 1. (a, b) SEM images of g-VB12 catalysts at different magnification. (c) N_2 adsorption and desorption isotherms of g-VB12. (d) The pore size distribution curve from the BJH method.

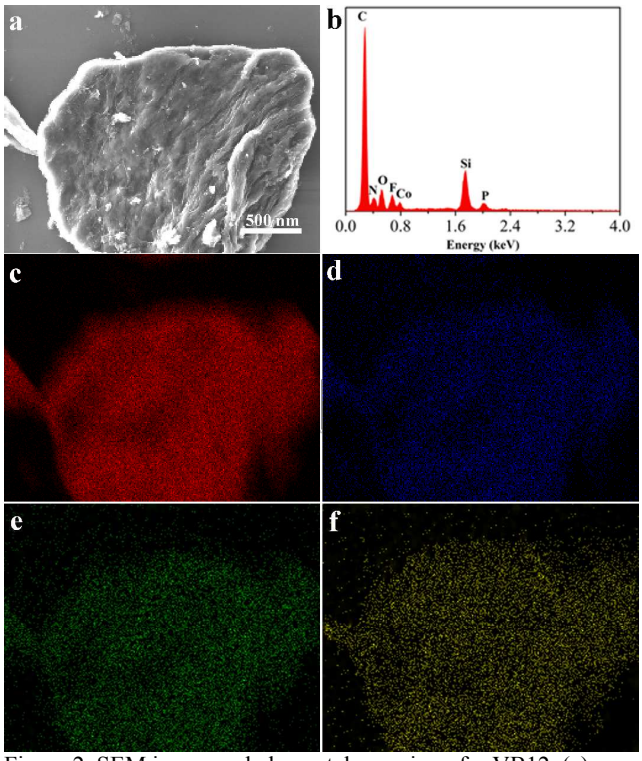

Figure 2. SEM image and elemental mapping of g-VB12. (a) Typical SEM photograph. (b) The EDX spectrum of g-VB12. (c-f) corresponding elemental mapping images of (c) C, (d) O, (e) N, (f) Co.

Energy-dispersive X-ray spectra (EDX) and elemental mapping analysis of the g-VB12 suggest the presence of C, N, Co, and O in the hybrids (Figure 2). It can be observed that the signals of Si and F come from the supporting silicon wafer and the Nafion solution, respectively. The possible contribution of trace residual P element to the ORR activity is excluded by previous reports.[28] The elemental mapping shows that both N and Co species are homogeneously distributed throughout the whole catalyst structure.

The containing elements and chemical state of the nitrogen and cobalt in the g-VB12 were further analyzed by X-ray photoelectron spectroscopy (XPS). The survey spectra in Figure 3a shows that C, N, O, and Co can be obviously detected. The high-resolution N1s spectra indicates the presence of three dominating signals of doping N, including pyridinic N at 398.5 eV, pyrolic N at 400.3 eV, and quaternary N at 401.5 eV. The peak centered at 398.5 eV should also include the contribution of N bonding to the cobalt (Co-N) on account of the little difference between the binding energy of Co-N and pyridinic N.[29]

In order to know the definite state of Co element in the g-VB12 composite, high-resolution transmission electron microscopy (HRTEM) inspection was performed. Metal-containing nanoparticles can hardly be observed from the HRTEM image (Figure S2). X-ray diffraction (XRD) pattern further proves the absence of crystalline metal/metal oxide phases (Figure S3). Therefore we deduce that the cobalt atoms exist in the coordinated state. High-resolution XPS spectra shows two peaks of Co2p3/2 at 781.2 and 779.6 eV, corresponding to N- and O-coordinated Co, respectively.[30] The latter might be attributed to the inevitable oxidation of trace Co by some released oxygen-

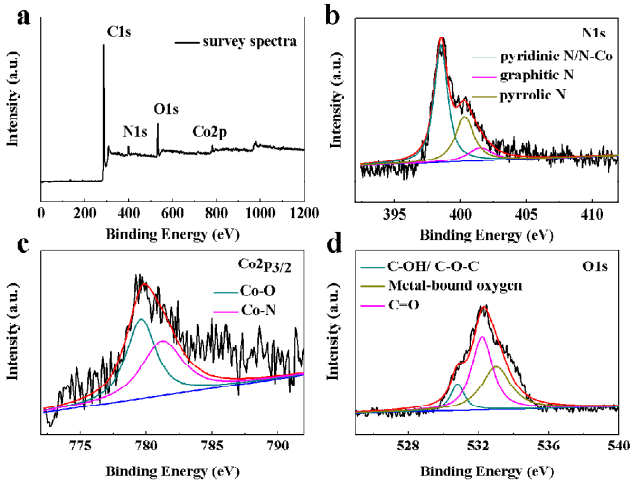

Figure 3. (a) XPS survey spectra of g-VB12. High resolution N1s XPS spectra (b), $Co2p_{3/2}$ spectra (c), and O1s spectra (d) of the g-VB12 catalyst.

containing groups which were not timely drain out during the pyrolysis. A small quantity of oxygen also exists in the composite, resulting from the incomplete reduction of graphene oxide. Although the exact structure of the active sites in the g-VB12 composite remains uncertain until now, there is a consensus that Co centers stabilized by N coordination (Co-Nx) act as the active sites in pyrolyzed VB12 during the ORR process.[15,28] In-depth study in previous reports supported the existence of a stable four-coordinated Co (□) compound acting as the active center.[25]

It was reported that during high-temperature pyrolysis reduction of graphene oxide, the resulting graphene was prone to be doped by N when there was suitable nitrogen source in this system.[10] From the EDX analysis (average value of three parallel measurements, see Table S1), the atom content in the as-synthesized g-VB12 composite is 12.36% for nitrogen and 1.85% for cobalt, respectively. The N/Co atom ratio in the g-VB12 composite is ca. 6.68, which is much higher than that of VB12/C (with a N/Co atom ratio of ca. 4.54, Table S1). Apart from the Co-Nx complex with a four N-to-Co coordination in the g-VB12 composite as mentioned above, there are still redundant N atoms doped to the special graphene skeleton during the pyrolysis process, which is further confirmed by the high-resolution N1s XPS spectra. Whereas carbon black acting as the support during the pyrolysis could not be easily doped by N and resulted in a relatively low N/Co ratio. N-doped graphene has been testified to be an efficient electrocatalyst in ORR as either the catalysts directly or carbon support to anchor catalysts.[8,10,31] Overall, the easily accessible three-dimensional mesoporous framework, the well dispersed Co-Nx species, together with the N doped graphene structure of the g-VB12 are highly beneficial to the electrocatalytic performance in the ORR process.

We first measured the electrocatalytic property of g-VB12 using cyclic voltammetry (CV) to gain insight into the ORR activity of the g-VB12 in N_2- and O_2- saturated 0.1 M aqueous KOH electrolyte solution at a scan rate of 10 mV s^{-1}. For comparison, commercial 20 wt % Pt on Vulcan carbon black (Pt/C from E-tek) was also tested under the same condition. As shown in Figure 4a, for the N_2-saturated solution, redox features are negligible for both g-VB12 and Pt/C. In contrast, for the O_2-saturated solution, the CV curve of g-VB12 exhibited a

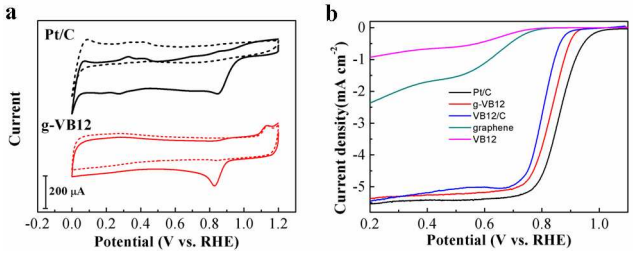

Figure 4. (a) CV curves of g-VB 12 and Pt/C in O_2- (dashed line) and N_2-saturated (solid line) 0.1 M KOH. (b) Comparison of the RDE polarization curves in O_2-saturated KOH at 1600 rpm.

pronounced cathodic ORR peak at 0.83 V with the onset potential of ca. 0.925 V. The oxygen reduction peak of g-VB12 is close to that of the commercial Pt/C, and the current densities of the two samples are also comparable. These results indicate the excellent intrinsic ORR performance of the g-VB12.

Subsequently, to further examine the electrocatalytic performance of g-VB12, linear sweep voltammetry (LSV) measurements were carried out in an O_2-saturated 0.1 M KOH electrolyte at a scan rate of 10 mV s^{-1} using rotating disk electrode (RDE). We first studied the ORR activity of the g-VB12 as a function of the pyrolysis temperature (600 °C, 700 °C, 800 °C). It was found that the best ORR activity is obtained at 700 °C, as revealed by the onset and half-wave potentials, as well as the diffusion-limiting current (Figure S4). Previous reports also demonstrated that the VB12 pyrolyzed at 700 °C exhibited the highest ORR activity, probably because an optimal balance of active site density, surface area and electron transfer ability was achieved after pyrolyzing at this temperature.[32] Figure 4b displays a set of characteristic ORR polarization curves of g-VB12, VB12/C, VB12, graphene, and commercial Pt/C modified RDEs. The unsupported pyrolyzed VB12 exhibits little ORR activity. Graphene obtained by heating at 700 °C also shows poor performance. The much more positive half-wave potential and larger diffusion-limiting current of g-VB12 catalyst than those of VB12 and graphene suggest the existence of synergetic effect between pyrolyzed VB12 and graphene in the composite. As shown in Figure 4b, the LSV polarization curve of g-VB12 exhibits an onset potential more positive than that of VB12/C. The half-wave potential of g-VB12 ($E_{1/2}$) is at 0.833 V, which is ca. 27 mV more positive than that of VB12/C, and only 30 mV negative shift compared with Pt/C catalyst. In addition, the diffusion-limiting current of g-VB12 is also comparable to that of Pt/C catalyst. The performances of g-VB12 are even comparable to those of some top reports concerning non-precious metal electrocatalysts in onset and half-wave potentials in alkaline electrolyte (Table S2), highlighting its high ORR activity.

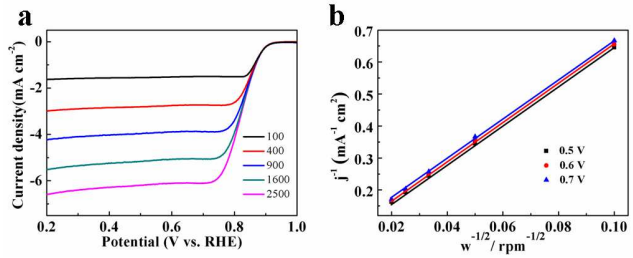

Figure 5. (a) ORR polarization curves for g-VB12 catalysts at the different rotation rates. (b) Koutecky-Levich plot for g-VB12 obtained from LSVs in (a) at different potentials.

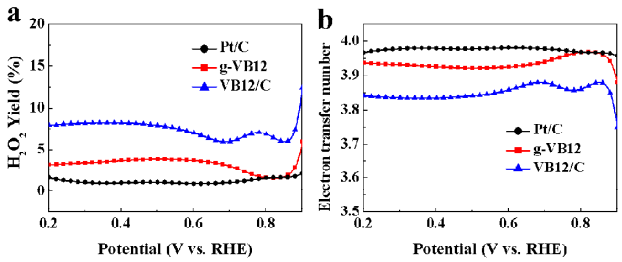

Figure 6. (a) Peroxide percentage and (b) electron transfer number of g-VB12 catalyst as a functions of the electrode potential.

The kinetics of electrochemical catalytic ORR performance on g-VB12 was also studied by RDE measurements. A set of ORR polarization curves recorded from 100 to 2500 rpm are displayed in Figure 5. The polarization curves show typical increasing currents at higher rotation speeds, which can be explained by shortened diffusion distance at high speeds. Koutecky-Levich (K-L) plots (j^{-1} vs. $\omega^{-1/2}$) derived from RDE tests are drawn at different potentials (0.5 V, 0.6 V and 0.7 V). The good linearity of the K-L plots and near parallelism of the fitting lines indicate the first-order reaction kinetics towards the concentration of dissolved oxygen and the similar ORR electron transfer number at different potentials.[33] The electron transfer number is calculated to be approaching 4 at the researched potentials from the slopes of K-L plots, demonstrating that the g-VB12 catalyzes the ORR process dominantly through a 4 electron transfer process. This result resembles to that of the ORR catalyzed by commercial Pt/C catalyst (n~4 for Pt/C, Figure S5).

Rotating ring disk electrode (RRDE) technique was also carried out to clearly verify the ORR electron transfer pathway by accurately detecting the amount of H_2O_2 generating at the Pt disk. The potential of the Pt ring electrode in the RRDE test is set at 1.5 V for detecting the peroxide species collected at the disk electrode. In the potential range between 0.2 V to 0.8 V, the H_2O_2 yield of g-VB12 remains below 4% (Figure 6a), corresponding to a high electron-transfer number of above 3.92 (Figure 6b). The electron transfer number varies little over the whole aforementioned potential range, emphasizing the ORR process of g-VB12 mainly through a four-electron mechanism.

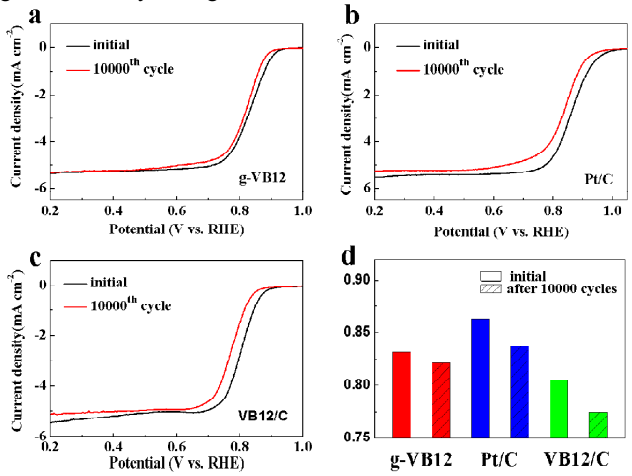

Figure 7. RDE polarization curves of the g-VB12 (a), Pt/C (b), and VB12/C (c) before and after 10000 potential cycles in O_2-saturated 0.1 M KOH. (d) Comparison of half-wave potentials ($E_{1/2}$) of the three catalysts before and after potential cycles.

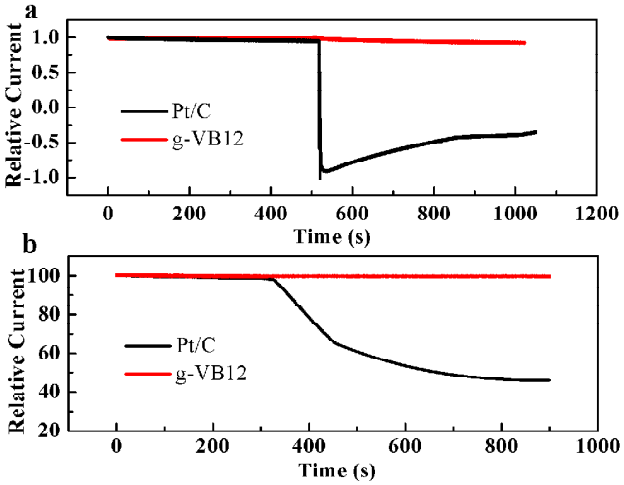

Figure 8. The chronoamperometric response of ORR at 0.8 V on g-VB12 and Pt/C electrodes in O_2-saturated 0.1 M KOH solution with the quick injection of 1 M methnol (a) and introduction of CO (b) at certain time during the test.

To clarify the dominant active centre of our g-VB12 catalyst for ORR, we have done the CN^- poisoning experiment with caution, as CN^- are known to coordinate strongly with some transition metal (such as Fe, Co, Cu) and ruin the Co-Nx centres (Figure S6)[34,35]. In the presence of CN^-, the ORR onset potential of the g-VB12 catalyst negatively shifted by more than 100 mV, with a decrease in the diffusion limiting current. The results clearly suggest that blocking of the Co sites by CN^- will lead to the distinct decrease of the activity of g-VB12 catalyst. A recent review has summarizes that apart from being an ORR catalyst itself, N-doped graphene can also act as an effective catalyst support during the ORR[10]. When acting as catalyst itself, N-doped graphene has good electrocatalytic property[36], but its activity is generally not as high as that of the g-VB12 catalyst especially in onset and half-wave potential in alkaline electrolyte.[36-39] while in the cases of more active catalysts supported by N-doped graphene, more active catalysts act as active sites and N-doped graphene can enhance the catalytic property[40-42]. From the CN^- poisoning experiment and literatures, we can conclude that Co-Nx was the dominant active site for ORR in the present study, while N-doped graphene acted as an effective support, and had a distinct enhancement in the activity and stability of Co-Nx supported on it.

We also assessed the durability of the g-VB12 using the accelerate durability tests by cycling the catalysts between 0.6 and 1.0 V at 50 mV s^{-1} in oxygen-saturated 0.1 M KOH. After 10000 continuous potential cycles, the half-wave potential ($E_{1/2}$) exhibits a small negative shift of 11 mV (Figure 7a), which outperforms most non-precious metal catalysts, including VB12/C electrocatalyst (30 mV, Figure 7c). The durability of g-VB12 also compares favourably with that of the commercial Pt/C (ca. 26 mV negative shift, Figure 7b). The half-wave potentials before and after 10000 potential cycles of g-VB12, VB12/C, and Pt/C are visually drawn up in Figure 7d, from which the comparison of activity and durability of the three samples can be easily obtained. It is believed that the durability of non-precious metal catalyst is highly correlated with the amount of peroxide releasing during the ORR.[43] The extremely low H_2O_2 yield of the g-VB12 would be beneficial to its electrochemical stability. We

also explore the in-depth reason for the ultra-high durability in consideration on the catalyst structure. Taking into account the similar composition of the g-VB12 composite and VB12/C, the remarkable enhancement in durability on the g-VB12 can be attributed to their unique structure. Specifically, the composite catalyst prepared in this study has a three-dimensionally interconnected mesoporous graphene framework. This well-confined structure can enhance the interfacial contact, suppress the structural collapse or active centers dissolution, and facilitate the transport of electron and reactant, and thus help to keep our g-VB12 far more stable than other VB12/C materials or commercial Pt/C.[7, 44, 45]

The g-VB12 catalyst was also exposed to some molecules for testing possible poisoning effect. An excellent catalytic selectivity for the cathode oxygen reduction reactions against fuel oxidation is significant for an effective ORR electrocatalyst in fuel cell application, especially when using small-molecule organic fuels, such as methanol, which may cross over through the polymer electrolyte membrane from anode to cathode, and lower the whole cell performance.[46] Both g-VB12 and Pt/C were subjected to testing the possible crossover in the presence of 1 M methanol (Figure 8a). After adding methanol to the electrolyte solution, the g-VB12 maintains unchanged current response whereas the current response of Pt/C jumps to positive values immediately owing to the occurrence of methanol oxidation on the Pt/C. CO poisoning is also one of the major issues in current fuel cell technology,[47] so the two catalysts are further exposed to 10 % (v/v) CO in O_2 to test their tolerance to CO poisoning effect. As shown in Figure 8b, the g-VB12 electrode is insensitive to CO whereas the Pt/C electrode is rapidly poisoned under the same condition. These results indicate that the g-VB12 has a higher selectivity toward ORR and better methanol and CO tolerance than the commercial Pt/C.

Experimental section

Materials.

The Cyanocobalamin (Vitamin B12) was purchased from Sinopharm Chemical Reagent Co., Ltd. The 20 % E-TEK Pt/C was bought from Alfa Aesar. The Vulcan XC-72 carbon supports was obtained from Cabot Corporation (USA). Graphite powder was purchased from Tianjin Guangfu Fine Chemical Research Institute. Unless otherwise stated, other reagents were of analytical grade and used as received. Aqueous solutions were prepared with double-distilled water from a Millipore system (>18 MΩ cm).

Sample preparation.

Graphene oxide (GO) was synthesized from graphite powder following a modified Hummers' method. The typical three-dimensional mesoporous g-VB12 was prepared as follows: 20 mg VB12 was added to 5 mL of GO aqueous solution (ca. 4 mg mL^{-1}) under vigorous stirring. After freeze-drying of the mixture, the as-prepared foam was then pyrolyzed under flowing Ar with a heating rate of 5 °C min^{-1} to desired temperatures (600-800 °C) and the temperature was kept for 2h. The g-VB12 electrocatalyst was finally obtained after the furnace was cooled to room temperature. For comparison, pyrolyzed VB12 supported on carbon black (Vulcan XC-72R) was also prepared under the same condition excepting carbon black aqueous dispersion was used instead of GO solution.

Characterizations.

Scanning electron microscopy (SEM) and energy-dispersive X-ray spectroscopy (EDX) were performed on a field emission scanning electron microscope (FE-SEM, XL30ESEM-FEG). High-resolution transmission electron microscopy (HRTEM) images were carried out on a JEM-2100 microscope operated at 200 kV. The Brunauer-Emmett-Teller (BET) surface area was obtained from 77 K N_2 sorption isotherms using ASAP 2020 instrument. XPS measurement was performed on an ESCALAB-MKII spectrometer (VG Co., United Kingdom) with Al Kα X-ray radiation as the X-ray source for excitation. X-ray diffraction (XRD) spectra were obtained by a D8 ADVANCE (Germany) using Cu-Kα radiation with a Ni filter (λ = 1.5406 Å at 30 kV and 15 mA).

Electrochemical Measurements.

Cyclic voltammograms (CVs) were obtained with a CHI 660A electrochemical workstation in a conventional 3-electrodes system. The working electrode was a 3 mm glassy carbon electrode (GCE) covered with the catalyst samples. Platinum coils and saturated calomel electrode (0.242 V vs. NHE) were used as the counter and the reference electrode, respectively. All electrode potentials in this work were converted to the RHE (reversible hydrogen electrode) scale without special description. The rotating disk electrode (RDE, d=5 mm) and rotating ring disk electrode (RRDE, with a glassy carbon disk of 5.61 mm in diameter and a ring made of Pt) tests were measured on a MSR Electrode Rotator with CE Mark from PINE Instrument. The Pt ring potential was set at 1.5 V (vs. RHE) in the RRDE tests. The electrolyte used in the ORR test was nitrogen or oxygen-saturated 0.1 M KOH, and the scan rate was 10 mV s^{-1}. Before use, the working electrodes were carefully polished to a mirror finish with 1.0-, 0.3-, and 0.05- μm alumina slurries, successively and cleaned by ultrasonication.

The catalyst ink was prepared by blending the catalyst powder (5 mg) with 300 μL water and 110 μL isopropanol and 100 μL Nafion aqueous solution (0.5 wt %) and then suffered to ultrasonication. 12 μL of the catalyst ink was then pipetted onto the RDE surface, leading to a catalyst loading of 0.6 mg cm^{-2}. The preparation of the VB12/C working electrode was just like that of the g-VB12 except g-VB12 was replaced by VB12/C. For the commercial Pt catalyst supported on Vulcan carbon black (Pt/C, 20 wt % Pt), the working electrode was prepared as follows: 2 mg Pt/C was dispersed in 970 μL ethanol and 50 μL Nafion solution (0.5 wt %) by sonication. 10 μL homogeneous ink was then dropped onto the GCE surface, leading to a Pt loading of 20 μg cm^{-2}. For the tests based on GCE and RRDE, certain amount of catalyst inks were added, leading to the same catalysts loading as that of the RDE per surface area.

To obtain the electron transfer number (n), the RDE electrode was scanned cathodically with varying rotating speed from 100 to 2500 rpm in O_2-saturated 0.1 M KOH aqueous solution. Koutecky-Levich plots (j^{-1} vs. $\omega^{-1/2}$) were analyzed at various potentials. The electron transfer number can be calculated from the slops of Koutecky-Levich equations as follows:[48]

$$\frac{1}{j} = \frac{1}{j_k} + \frac{1}{B\omega^{0.5}} \quad (1)$$

$$B = 0.2nF(D_0)^{2/3}v^{-1/6}C_0 \quad (2)$$

where j is the measured current density, j_k is the kinetic current density, ω is the electrode rotating rate, n represents the number of electron transferred per oxygen molecule, F is the Faraday constant (F=96485 C mol^{-1}), D_0 is the diffusion coefficient of O_2 in 0.1 M KOH (1.9×10^{-5} cm^2 s^{-1}), v is the kinematic viscosity of the electrolyte (0.01 cm^2 s^{-1}), and C_0 is the bulk concentration of O_2 (1.2×10^{-6} mol cm^{-3}).[49] The constant 0.2 is used when the rotation speed is expressed in rpm.

For the RRDE measurements, the percentage of H_2O_2 and the electron transfer number were determined by the following equations:

$$H_2O_2\% = 200\times\frac{I_r/N}{I_d + I_r/N} \quad (3)$$

$$n = 4\times\frac{I_d}{I_d + I_r/N} \quad (4)$$

where I_d is the disk current, I_r is the ring current, and N is the current collection efficiency of the Pt ring. N was determined to be 0.38 from the reduction of $K_3Fe[CN]_6$, well consistent with the manufacturer's value (0.37).

Conclusions

In summary, we have successfully designed a Co-Nx complex on mesoporous 3D N-doped graphene with outstanding ORR performance for alkaline fuel cells. It is notable that this work offers a facile and low-cost way to synthesize high performance carbon supported transition metal/nitrogen (M-Nx/C) non-precious metal electrocatalyst, whose research stagnated these years after several decades of evolution. This novel g-VB12 possesses excellent electrocatalytic property for ORR in alkaline electrolytes, comparable to fresh commercial Pt/C in activity but exceeding Pt/C in durability and anti-poison ability in half-cell test. This catalyst also outperforms the conventional pyrolyzed VB12 supported on Vulcan carbon black in both activity and durability. The outstanding ORR performance of the g-VB12 catalyst is strongly associated with its homogeneous distribution of numerous Co-Nx active sites. In addition, the well-defined mesoporous 3D structure, relatively high surface area, and N doping to the graphene skeleton are also favorable for the ORR activity. Low cost raw materials, facile preparation method, and satisfying ORR performance are simultaneously achieved, making this g-VB12 a promising non-precious metal cathode catalyst for alkaline fuel cells.

Acknowledgements

The authors are most grateful to the NSFC, China (No. 21225524, 21175130, 21105096 and 21205112) and the Department of Science and Techniques of Jilin Province (No. 201105031, 20120308 and 201215091) for their financial support.

Notes and references

[a] *State Key Laboratory of Electroanalytical Chemistry, Changchun Institute of Applied Chemistry, Changchun 130022, Jilin, China. Email: lniu@ciac.ac.cn and ybao@ciac.ac.cn; Tel:+86 431 85262425*
[b] *Engineering Laboratory for Modern Analytical Techniques, Changchun Institute of Applied Chemistry, Changchun 130022, Jilin, China*
[c] *University of Chinese Academy of Sciences, Beijing, 100039, China*
† Electronic Supplementary Information (ESI) available: [details of any supplementary information available should be included here]. See DOI: 10.1039/b000000x/

1 H. A. Gasteiger and N. M. Marković, *Science*, 2009, **324**, 48-49.
2 M. Prabu, K. Ketpang and S. Shanmugam, *Nanoscale*, 2014, **6**, 3173-3181.
3 Y. Bing, H. Liu, L. Zhang, D. Ghosh and J. Zhang, *Chem. Soc. Rev.*, 2010, 39, 2184-2202.
4 D. S. Su and G. Sun, *Angew. Chem. Int. Ed.*, 2011, **50**, 11570-11572.
5 A. Morozan, B. Jousselme and S. Palacin, *Energy Environ. Sci.*, 2011, **4**, 1238-1254.
6 S. Guo, S. Zhang, L. Wu and S. Sun, *Angew. Chem. Int. Ed.*, 2012, **51**, 11770-11773.
7 Z.-S. Wu, S. Yang, Y. Sun, K. Parvez, X. Feng and K. Muellen, *J. Am. Chem. Soc.*, 2012, **134,** 9082-9085.
8 Y. Liang, Y. Li, H. Wang, J. Zhou, J. Wang, T. Regier and H. Dai, *Nat. Mater.*, 2011, **10**, 780-786.
9 Y. Zheng, Y. Jiao, L. Ge, M. Jaroniec and S. Z. Qiao, *Angew. Chem. Int. Ed.*, 2013, **52**, 3110-3116.
10 H. Wang, T. Maiyalagan and X. Wang, *ACS Catal.*, 2012, **2**, 781-794.
11 K. Gong, F. Du, Z. Xia, M. Durstock and L. Dai, *Science*, 2009, **323**, 760-764.
12 S. Chen, J. Y. Bi, Y. Zhao, L. J. Yang, C. Zhang, Y. W. Ma, Q. Wu, X. Z. Wang and Z. Hu, *Adv. Mater.*, 2012, **24**, 5593-5597.
13 A. Morozan, S. Campidelli, A. Filoramo, B. Jousselme and S. Palacin, *Carbon*, 2011, **49**, 4839-4847.
14 C. Zhang, R. Hao, H. Yin, F. Liu and Y. Hou, *Nanoscale*, 2012, **4**, 7326-7329.
15 Y. Jiang, Y. Lu, X. Lv, D. Han, Q. Zhang, L. Niu and W. Chen, *Acs Catal.*, 2013, **3**, 1263-1271.
16 Z. Chen, D. Higgins, A. Yu, L. Zhang and J. Zhang, *Energy Environ. Sci.*, 2011, **4**, 3167-3192.
17 C. W. B. Bezerra, L. Zhang, H. Liu, K. Lee, A. L. B. Marques, E. P. Marques, H. Wang and J. Zhang, *J. Power Sources*, 2007, **173**, 891-908.
18 R. Jasinski, *Nature*, 1964, **201**, 1212-1213.
19 L. Zhang, J. J. Zhang, D. P. Wilkinson and H. J. Wang, *J. Power Sources*, 2006, **156**, 171-182.
20 R. Chen, H. Li, D. Chu and G. Wang, *J. Phys. Chem. C*, 2009, **113**, 20689-20697.
21 D. A. Scherson, S. L. Gupta, C. Fierro, E. B. Yeager, M. E. Kordesch, J. Eldridge, R. W. Hoffman and J. Blue, *Electrochim. Acta,* 1983, **28**, 1205-1209.
22 L. N. Ramavathu, K. K. Maniam, K. Gopalram and R. Chetty, *J. Appl. Electrochem.*, 2012, **42**, 945-951.
23 S. Gupta, D. Tryk, I. Bae, W. Aldred and E. Yeager, *J. Appl. Electrochem.*, 1989, **19**, 19-27.
24 M. Lefevre, E. Proietti, F. Jaouen and J.-P. Dodelet, *Science*, 2009, **324**, 71-74.
25 S.-T. Chang, C.-H. Wang, H.-Y. Du, H.-C. Hsu, C.-M. Kang, C.-C. Chen, J. C. S. Wu, S.-C. Yen, W.-F. Huang, L.-C. Chen, M. C. Lin and K.-H. Chen, *Energy Environ. Sci.*, 2012, **5**, 5305-5314.
26 Y. H. Xue, J. Liu, H. Chen, R. G. Wang, D. Q. Li, J. Qu and L. M. Dai, *Angew. Chem. Int. Ed.*, 2012, **51**, 12124-12127.
27 Y. Zhao, C. G. Hu, Y. Hu, H. H. Cheng, G. Q. Shi and L. T. Qu, *Angew. Chem. Int. Ed.*, 2012, **51**, 11371-11375.
28 H. W. Liang, W. Wei, Z. S. Wu, X. L. Feng and K. Mullen, *J. Am. Chem. Soc.*, 2013, **135**, 16002-16005.

29 G. Wu, C. M. Johnston, N. H. Mack, K. Artyushkova, M. Ferrandon, M. Nelson, J. S. Lezama-Pacheco, S. D. Conradson, K. L. More, D. J. Myers and P. Zelenay, *J. Mater. Chem.*, 2011, **21**, 11392-11405.

30 G. Wu, Z. W. Chen, K. Artyushkova, F. H. Garzon and P. Zelenay, *ECS Transactions* 2008, **16**, 159-170.

31 D. Geng, Y. Chen, Y. Chen, Y. Li, R. Li, X. Sun, S. Ye and S. Knights, *Energy Environ. Sci.*, 2011, **4**, 760-764.

32 S. T. Chang, C. H. Wang, H. Y. Du, H. C. Hsu, C. M. Kang, C. C. Chen, J. C. S. Wu, S. C. Yen, W. F. Huang, L. C. Chen, M. C. Lin and K. H. Chen, *Energy Environ. Sci.*, 2012, **5**, 5305-5314.

33 Y. Y. Liang, Y. G. Li, H. L. Wang, J. G. Zhou, J. Wang, T. Regier and H. J. Dai, *Nat. Mater.*, 2011, **10**, 780-786.

34 S. Gupta, C. Fierro, and E. Yeager, *J. Electroanal. Chem.*, 1991 **1-2**, 239-250.

35 M.S. Thorum, J.M. Hankett, and A.A. Gewirth, *J. Phys. Chem. Lett.*, 2011, **4**, 295-298.

36 L.T. Qu, Y. Liu, J.B. Baek, and L.M. Dai, *ACS nano*, 2010, **3**, 1321-1326.

37 H. Zhao, K.S. Hui, and K.N. Hui, *Carbon*, 2014, 1-9.

38 Z.Y. Lin, G.H. Waller, Y. Liu, M.L. Liu, and C.P. Wong, *Nano Energy*, 2013, **2**, 241-248.

39 Y. Li, Y. Zhao, H.H. Cheng, Y. Hu, G.Q. Shi, L.M. Dai, and L.T. Qu, *J. Am. Chem. Soc.*, 2012, **1**, 15-18.

40 R.I. Jafri, N. Rajalakshmi, and S. Ramaprabhu, *J. Mater. Chem.*, 2010, **34**, 7114-7117.

41 C.W. Tsai, M.H. Tu, C.J. Chen, T.F. Hung, R.S. Liu, W.R. Liu, M.Y. Lo, Y.M. Peng, L. Zhang, J.J. Zhang, D.S. Shy, and X.K. Xing, *Rsc Advances*, 2011, **7**, 1349-1357.

42 C.Z. Zhang, R. Hao, H. Yin, F. Liu, and Y.L. Hou, *Nanoscale*, 2012, **23**, 7326-7329.

43 F. Jaouen, E. Proietti, M. Lefevre, R. Chenitz, J.-P. Dodelet, G. Wu, H. T. Chung, C. M. Johnston and P. Zelenay, *Energy Environ. Sci.*, 2011, **4**, 114-130.

44 J. Liang, Y. Zheng, J. Chen, J. Liu, D. Hulicova-Jurcakova, M. Jaroniec and S. Z. Qiao, *Angew. Chem. Int. Ed.*, 2012, **51**, 3892-3896.

45 Y. Jiang, X. Zhang, C. Shan, S. Hua, Q. Zhang, X. Bai, L. Dan and L. Niu, *Talanta*, 2011, **85**, 76-81.

46 Y. M. Tan, C. F. Xu, G. X. Chen, N. F. Zheng and Q. J. Xie, *Energy Environ. Sci.*, 2012, **5**, 6923-6927.

47 G. Ma, R. Jia, J. Zhao, Z. Wang, C. Song, S. Jia and Z. Zhu, *J. Phys. Chem. C*, 2011, **115**, 25148-25154.

48 L. R. Faulkner, A. J. Bard, *Electrochemical Methods: Fundamentals and Applications*, 2001, 2nd edition.

49 W. Chen and S. Chen, *Angew. Chem. Int. Ed.*, 2009, **48**, 4386-4389.